

Stability of an ionization front in Bondi accretion

Eric Keto¹★ and Rolf Kuiper²★

¹*Institute for Theory and Computation, Harvard College Observatory, 60 Garden St, Cambridge, MA 02138, USA*

²*Institut für Theoretische Astrophysik, Zentrum für Astronomie der Universität Heidelberg, Albert-Ueberle-Straße 2, D-69120 Heidelberg, Germany*

Accepted 2021 October 9. Received 2021 October 9; in original form 2021 August 4

ABSTRACT

Spherical Bondi accretion is used in astrophysics as an approximation to investigate many types of accretion processes. Two-phase accretion flows that transition from neutral to ionized have observational support in high-mass star formation, and have application to accretion flows around any ionizing source, but the hydrodynamic stability of two-phase Bondi accretion is not understood. With both semi-analytic and fully numerical methods, we find that these flows may be stable, conditionally stable, or unstable depending on the initial conditions. The transition from an R-type to a D-type ionization front plays a key role in conditionally stable and unstable flows.

Key words: hydrodynamics – stars: formation.

1 INTRODUCTION

Shortly after Bondi’s explanation (Bondi 1952) of his eponymous accretion flow, Mestel (1954) described a Bondi accretion flow through a static ionization front as might exist around a compact ionizing source. The Rankine–Hugoniot equations for the discontinuity across the ionization front allow solutions for supersonic or subsonic relative velocities of the front with respect to the neutral accretion flow. However, there is a range of relative velocities, approximately around the sound speed of the ionized gas, for which the jump conditions result in an unphysical square root of a negative number. Thus, at that time, the applicability of Mestel’s model was not clear. A year later, Savedoff & Greene (1955) resolved the problematic jump conditions with a double discontinuity made up of a shock front preceding the ionization front.

Observations of radio recombination lines from the ultracompact H II region, G10.6-04, matching the morphology and inward velocity of the surrounding molecular accretion flow (Keto 2002a,b) suggest the relevance of Mestel’s model with a molecular accretion flow passing through the ionization front at the H II region boundary and continuing to the star as an ionized accretion flow. This interpretation recasts the role of an H II region around a massive accreting protostar from a disruptor to a participant in the accretion flow. The model is also applicable to rotationally flattened accretion flows, where the accretion is confined about the mid-plane of the rotating system (Keto 2007).

The temporal evolution of a two-phase accretion flow is described in Keto (2002b) as a continuous transition through steady-state solutions parametrized by the ionizing luminosity or equivalently the position of the ionization front. This description is adequate assuming that the time-scale for the ionized flow to adjust to a new steady-state solution, the fluid-crossing time, is short compared to the time-scale for changes in the velocity of the ionization front.

However, the velocity of the ionization front depends on the ionizing luminosity and the ionized and neutral gas densities (Section 2.2). These are both independent of the gas velocity in the sense that Bondi’s solution contains an arbitrary scaling factor for the density. Therefore, the assumption of a steady-state flow in the ionized gas is not guaranteed. Recent numerical hydrodynamic studies found no stable solutions and suggested that the dynamics in this model may be inherently unstable (Vandenbroucke et al. 2019).

Owing to its simplicity and flexibility rather than astrophysical realism,¹ the spherically symmetric Bondi accretion flow has been a useful approximation for investigations of a wide range of accretion phenomena. The stability of two-phase Bondi accretion flows is therefore worth understanding in order to extend the applicability of this widely used approximation.

In this paper, we revisit the stability of an ionization front in a Bondi accretion flow through two different numerical methods. We follow Keto (2020) and use the method of characteristics to solve the partial differential equation (PDE) for time-dependent Bondi accretion within the H II region as a system of coupled ordinary differential equations (ODEs; Section 2). We also model the entire accretion flow from neutral to ionized, passing through the ionization front, with a numerical hydrodynamic simulation gridded in spherical geometry appropriate to the problem (Section 3).

In addition to the unstable solutions found in Vandenbroucke et al. (2019), we find stable solutions with damped oscillations and conditionally stable solutions with oscillations of limited amplification. The behaviour depends on the relationship between two time-scales: the time-scale for the H II region to change density, essentially the fluid-crossing time; and the time-scale for the ionization front to move to the new position of radiative equilibrium with the new density. The oscillations result as the front overshoots its equilibrium position.

¹For example, both the self-gravity and angular momentum of the accretion flow must be negligible.

* E-mail: eketo@cfa.harvard.edu (EK); kuiper@uni-heidelberg.de (RK)

2 SOLUTION BY ORDINARY DIFFERENTIAL EQUATIONS

2.1 Bondi accretion

Following Bondi (1952) and Parker (1958), the Euler equation in spherical symmetry for an isothermal gas with $\partial P / \partial \rho = a^2$ for sound speed, a , and a gravitational force from a constant mass, M , is (Keto 2020)

$$\frac{\partial \tilde{u}}{\partial \tilde{t}} = -\tilde{u} \frac{\partial \tilde{u}}{\partial \tilde{x}} - \frac{a^2}{\tilde{\rho}} \frac{\partial \tilde{\rho}}{\partial \tilde{x}} - \frac{GM}{\tilde{x}^2}, \quad (1)$$

where the tilde indicates a variable with dimensional units. This can be written in non-dimensional form with the definitions as

$$\tilde{x} = \left(\frac{GM}{a^2} \right) x, \quad \tilde{u} = au, \quad \tilde{t} = \left(\frac{GM}{a^3} \right) t, \quad \text{and} \quad \tilde{\rho} = \tilde{\rho}_0 \rho, \quad (2)$$

where $\tilde{\rho}_0$ is an arbitrary density. With these substitutions, equation (1) becomes

$$\frac{\partial u}{\partial t} = -u \frac{\partial u}{\partial x} - \frac{1}{\rho} \frac{\partial \rho}{\partial x} - \frac{1}{x^2}. \quad (3)$$

The density may be eliminated with the help of the non-dimensional continuity equation

$$\rho = \lambda x^{-2} u^{-1}, \quad (4)$$

where λ is the accretion rate. Then,

$$\frac{\partial u}{\partial t} = \left(\frac{1}{u} - u \right) \frac{\partial u}{\partial x} + \left(\frac{2}{x} - \frac{1}{x^2} \right). \quad (5)$$

In steady state, the time derivative on the left-hand side is zero, and the variables can be separated and integrated,

$$\mathcal{L} = \log |u| - \frac{1}{2} u^2 + 2 \log |x| + \frac{1}{x}. \quad (6)$$

In non-dimensional units, the constant of integration $\mathcal{L} = \log \lambda$ is equivalent to the energy and with a simple non-linear scaling to the mass accretion rate.

There is only one solution that transitions from subsonic to supersonic, the Bondi accretion flow with $\mathcal{L} = \mathcal{L}_C = 3/2 - 2 \log 2$. This solution passes through a critical point, $(x_c, u) = (\frac{1}{2}, 1)$ or $(\tilde{x}, \tilde{u}) = (GM/(2a^2), a)$. The coefficients (equations 2) used for the non-dimensional scaling are then, respectively, in the order listed, twice the radial distance of the transonic critical point, the sound speed, and twice the sound crossing time to the critical point. The density has been eliminated from the solution, and its scaling is arbitrary.

2.2 Ionization

The neutral accretion flow with velocity, $u_1(x)$, follows the unique transonic steady-state solution until it reaches the ionization front at position $x_f(t)$. Here, the flow is ionized, slowed down, and compressed and then follows a solution of the PDE (5), for velocity $u(x, t)$, and energy constant,

$$\mathcal{L} = \left(\frac{1}{x_f} + 2 \log x_f \right) - \left(\frac{1}{2} u_2^2(x_f) - \log |u_2(x_f)| \right), \quad (7)$$

where $u_2(x_f)$ is the velocity of the ionized gas at the position of the front, x_f .

In the following, the subscripts 1 and 2 indicate the neutral and ionized sides of the front, respectively, and \hat{u} a relative velocity of the gas with respect to the front, $\hat{u} = \dot{x}_f - u$, assuming that the gas

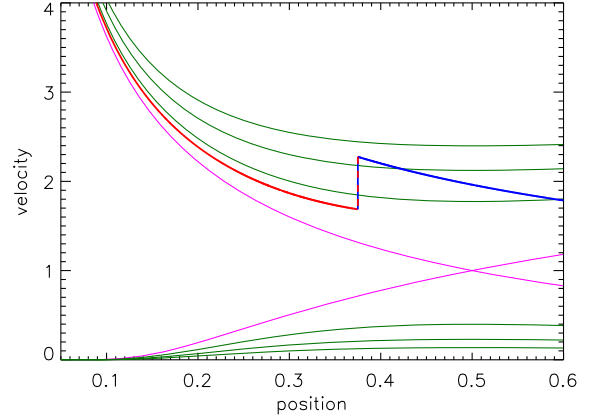


Figure 1. Velocity, u , as a function of position, x , in non-dimensional units scaled on the sound speed of the ionized gas. The pink lines show the transonic Bondi accretion flow and the Parker wind, crossing at the critical point $(x_c, u) = (1/2, 1)$. The green lines show some examples of subsonic and supersonic steady-state solutions. The blue and red lines show the initial conditions. The neutral flow (blue line) passes through the ionization front to continue inwards as an ionized accretion flow (red line). The ionization front is at position $3/8$.

velocity is negative for accretion. Then the relative velocity, \hat{u}_2 , is found from the Rankine–Hugoniot or jump conditions for continuity and momentum in non-dimensional form,

$$\rho_2 \hat{u}_2 = \rho_1 \hat{u}_1, \quad (8)$$

$$\rho_2 (1 + \hat{u}_2^2) = \rho_1 (\beta^2 + \hat{u}_1^2), \quad (9)$$

where $\beta = a_1/a_2$, and the non-dimensional scaling coefficients (equations 2) are defined with sound speed, a_2 . The jump conditions are combined,

$$1 + \hat{u}_1^2 \left(\frac{\rho_1}{\rho_2} \right)^2 - (\beta^2 + \hat{u}_1^2) \left(\frac{\rho_1}{\rho_2} \right) = 0, \quad (10)$$

and solved as a quadratic in the ratio, ρ_1/ρ_2 . The velocity \hat{u}_2 in terms of the known velocity \hat{u}_1 is

$$\hat{u}_2 = \eta \pm (\eta^2 - 1)^{1/2} \quad (11)$$

with

$$\eta = \frac{1}{2\hat{u}_1} (\beta^2 + \hat{u}_1^2). \quad (12)$$

The positive branch, conventionally called R-type, applies when the relative velocity, \hat{u}_1 , is supersonic, $\hat{u}_1 \geq u_R = 1 + \sqrt{1 - \beta^2} \approx 2$, and the negative branch, D-type, when subsonic, $\hat{u}_1 \leq u_D = 1 - \sqrt{1 - \beta^2} \approx \beta^2/2$. Relative velocities between u_D and u_R result in an unphysical negative argument of the square root in equation (11). The classification of ionization fronts is explained more fully in Shu (1991) or Spitzer (1978). The initial conditions are shown in Fig. 1.

2.3 Velocity of the ionization front

The velocity of the ionization front is set by the requirement of equality between the number of neutral atoms flowing into the front and the number of ionizing photons arriving at the front, both per unit time. The former depends on the relative velocity of the front and the neutral accretion flow, as well as the neutral density. The latter depends on the stellar rate of emission, \tilde{J}_* , less the rate of

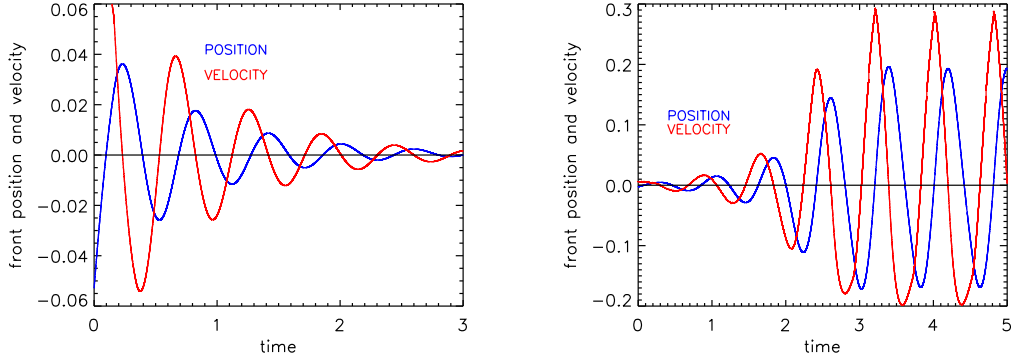


Figure 2. Velocity of the ionization front (red) and its position about equilibrium (blue), both shown relative to their respective equilibria and both in non-dimensional units. The initial position of the front is $3/8$ (left-hand panel) and $7/16$ (right-hand panel) and initially out of equilibrium with the stellar flux by 2 percent (left-hand panel) and 0.1 percent (right-hand panel). The amplitudes of the oscillations are limited as shown in the figure (right-hand panel) and continue at this level indefinitely.

recombinations in the H II region.

$$\left(\frac{d\tilde{x}_f}{dt} - \tilde{u}_1(\tilde{x}_f) \right) r \pi \tilde{x}_f^2 \frac{\tilde{\rho}_1(\tilde{x}_f)}{m_H} = \tilde{J}_* - \int_{\tilde{x}_*}^{\tilde{x}_f} \alpha \frac{\tilde{\rho}^2(\tilde{x}')}{m_H^2} 4\pi \tilde{x}'^2 d\tilde{x}', \quad (13)$$

where m_H is the mass of the hydrogen atom and the type-I recombination rate coefficient is $\alpha = 3 \times 10^{-13} \text{ cm}^3 \text{ s}^{-1}$. Ionization equilibrium is explained more fully in Shu (1991) or Spitzer (1978).

This equation can be written in non-dimensional form as

$$(\dot{x}_f - u_1(x_f)) x_f^2 \rho_1(x_f) = J_* - \int_{x_*}^{x_f} \rho^2 x'^2 dx' \quad (14)$$

or using the continuity equation (4) to eliminate the density as

$$(\dot{x}_f - u_1(x_f)) = \frac{u_1(x_f)}{\lambda} \left(J_* - \lambda^2 \int_{x_*}^{x_f} u^{-2}(x') x'^{-2} dx' \right). \quad (15)$$

In deriving the non-dimensional form, we set the density scaling coefficient in equation (2),

$$\left(\frac{m_H}{\alpha \rho_0} \right) \left(\frac{a^3}{GM} \right) = 1. \quad (16)$$

The two terms in parentheses are the ratio of the recombination time to the crossing time. Also,

$$J_* = \left[\frac{1}{a} \frac{1}{4\pi} \left(\frac{a^2}{GM} \right) \frac{m_H}{\rho_0} \right] \tilde{J}_*. \quad (17)$$

The right-hand side shows the ratio of the rate of ionizing photons from the star to the rate of neutral atoms through the critical point of the ionized Bondi accretion flow.

2.4 Time-dependent solution

The time-dependent evolution can be calculated from the PDE for the Bondi accretion flow (5), combined with the equation for the velocity of ionization front (15). Following the method of characteristics as explained in Keto (2020), the PDE may be converted into two first-order ODEs,

$$\frac{dx}{dt} = u - \frac{1}{u} \quad (18)$$

$$\frac{du}{dt} = \frac{2}{x} - \frac{1}{x^2}, \quad (19)$$

to be solved with initial values, $u(t, x) = u_0(x)$ at $t = 0$. With equation (15) for the position of the ionization front and its initial

condition, we have a system of three coupled ODEs. The neutral flow upstream of the H II boundary layer, either a simple ionization front or a combination of an ionization and a shock front, is independent of time, and we solve only for the ionized portion of the accretion flow and the motion of the front. Our numerical hydrodynamic simulations described later in Section 3 model the flow in the ionized zone and in both the pre- and post-shock neutral zones.

The system of coupled ODEs is an initial value problem (IVP), whereas we want to solve a boundary value problem (BVP) for the flow between the surface of the star and the time-dependent position of the ionization front. Accordingly, at each time-step, we remove from the calculation the characteristics represented by equation (18) that are advected past the inner boundary, and we add new characteristics to represent the gas flowing inwards through the outer boundary. The initial velocities for the new characteristics are determined from equation (11) for the combined jump conditions. Example solutions with damped and amplified oscillations are shown in Fig. 2.

2.5 Explanation

The oscillations are damped or amplified depending on the relationship between the phase of the oscillations of the velocity of the front and the phase of the oscillations of its position. The chain of causality involves several steps. The accretion flow is supersonic, and downstream changes in the ionized portion of the flow do not propagate to the ionization front. The neutral flow upstream is steady by assumption. The movement of the ionization front is therefore determined by the ionization balance, which depends on the ionized gas density through the total recombination rate expressed by the integral in equation (14).

The complexity arises because the motion of the front to establish a new equilibrium changes the relative velocity of the front with respect to the steady, neutral flow and thereby the compression across the front and the density of the gas entering the H II region. However, equilibrium requires a static front. Therefore, the ionized density entering the H II region through the moving front is not the density required for equilibrium. Advection then propagates this non-equilibrium density through the H II region, affecting the density-dependent recombination rate, the ionizing flux at the front, and in turn the velocity of the front. Generally, the front position overshoots its equilibrium, resulting in oscillations around the equilibrium position.

If the front is initially relatively close to the star, i.e. the H II region is small compared to the Bondi transonic radius (e.g. $x_f/x_c = 3/8$ and $1/5$ in our example ODE and fully numerical solutions, respectively), then the advection time-scale is short, and the oscillations of the position of the front lag the oscillations in the velocity of the front. In this case, the overshoot works to dampen the oscillations, which decay relatively quickly to the equilibrium position. If the H II region is larger (e.g. $x_f/x_c = 7/16$ and $1/2$ in our example ODE and fully numerical solutions, respectively), the advection time-scale is longer, and the oscillations of the position of the front lead those of the velocity of the front, and the overshoot is amplified. Fig. 3 illustrates the two cases. The arrows point to locations on the figure, where it is easy to see that the oscillations of position and velocity are not quite 180° out of phase. In the case of damped oscillations, the change in the sign of the velocity occurs just after the front has reached its furthest deviation from equilibrium for each cycle, whereas the opposite occurs in the case of amplified oscillations. In the two cases, the time differences either work to dampen or amplify, respectively, the oscillation in the next cycle.

For any set of initial conditions, there is a critical radius for the initial position of the ionization front that determines whether the evolution is stable or unstable. However, the critical radius is not universal but depends on the initial conditions, in particular on the locations of the inner and outer boundaries. At least for the moment, this critical radius must be found numerically by following the evolution.

2.5.1 Development of stable oscillations

If the oscillations are amplified, an ionization front starting from an initial position where $\hat{u}_1 \geq u_R$ may evolve such that $\hat{u}_1 = u_R$ even if the ionizing flux, J_* , is held constant. This generally occurs in the phase of the oscillation cycle when the position of the front is accelerating inwards in the same direction as the accretion flow and reducing the relative velocity of the front and the flow. If the relative velocity, \hat{u}_1 , were to fall below the critical velocity, u_R , the argument of the square root in equation (11) would become negative, resulting in unphysical jump conditions across the ionization front. This situation is resolved by the development of a shock front on the upstream side of the ionization front as suggested by Savedoff & Greene (1955). An ionization front at the critical relative velocity, u_R , is equivalent to a double front consisting of a D-type ionization front with a coincident and co-moving isothermal shock. In this equivalence, the shock slows the neutral gas entering the ionization front to the relative velocity, u_D , according to the jump conditions across an isothermal shock,

$$\hat{u}_{1s} = \beta^2 / (u_1 - \dot{x}_s), \quad (20)$$

where \hat{u}_{1s} is the relative velocity of the neutral gas behind the shock front and \dot{x}_s is the velocity of the shock front.

Our ODE model consists of two zones, the undisturbed neutral accretion flow and the H II region, and does not include a post-shock, compressed, neutral layer. If we assume that the post-shock layer is thin so that $\hat{u}_{1f} \approx \hat{u}_{1s}$, then the ionization and shock fronts need not be coincident. If we further assume that the compression in the post-shock layer results in the minimum pressure required to move the shock front ahead of the ionization front at the minimum velocity required for allowable jump conditions, then the relative velocity of the ionized gas behind the ionization front remains at the critical value $\hat{u}_{2f} = 1$ as long as the relative velocity ahead of the shock front is within the range $u_D < \hat{u}_{1s} < u_R$.

Thus, during the phase of the oscillation when the H II boundary is moving inwards and the upstream relative velocities are within this range, $u_D < \hat{u}_{1s} < u_R$, the density of the ionized gas that enters the H II region decreases less than it does when the single ionization front structure is allowed. After a crossing time, this gas, now near the inner boundary, dominates the number of recombinations in the integral in equations (13)–(15) and drives the outward motion of the ionization front less than it would without the transition to a double-front discontinuity. Thus, if the initial conditions allow, the growth of the amplitudes of the oscillation is limited by the development of the double-front discontinuity.

The transition from an R-type to a D-type ionization front may not be dramatic. In our ODE solution, we find that the front may switch back and forth between critical and subcritical several times per oscillation cycle, suggesting that a dense post-shock neutral layer does not necessarily build up and persist, at least not for the initial conditions of our example solution.

To continue the explanation, we compare the evolution of the ionization front within a Bondi accretion flow with two different models. First, under the right conditions, a non-linearly damped harmonic oscillator can lead to conditionally stable oscillations. Secondly, the ionization front in the textbook model for the pressure-driven expansion of an H II region within a uniform-density gas also transitions from R-type to D-type, but the conditions at the H II region boundary are controlled in a different way (Spitzer 1978; Shu 1991).

2.5.2 Comparison with a non-linearly damped harmonic oscillator

While the evolution of the ionization front to conditionally stable oscillations is similar to that of a forced and damped harmonic oscillator leading to a limit cycle, the equation for the position and velocity of the ionization front is different. The equation for a harmonic oscillator has the general form

$$\ddot{x} + b(x)\dot{x} + cx = f(t), \quad (21)$$

where b , c , and f are arbitrary constants or functions. If the damping term is suitably non-linear, in particular, stronger at the extrema of the oscillations, the evolution may lead to a classic limit cycle with conditionally stable oscillations as in the well-known van der Pol oscillator. In contrast, equation (14) for the velocity of the ionization front is of the form

$$\dot{x} = g(x, t) \quad (22)$$

with a function g . The dependence on position is seen in the upper limit of the integral in equation (14) and also in the velocity of the neutral flow at the position of the front. The time dependences result from the advection of the density across the H II region and the position of the front. The time derivative of equation (14) for the acceleration of the front is of the form

$$\ddot{x} = h(\dot{x}, t). \quad (23)$$

This is, of course, different from that of a harmonic oscillator (equation 21) in that the function $h(\dot{x}, t)$ depends only on time and the time derivative of x . In particular, the restoring force proportional to x is missing. A simple ODE for the acceleration of the ionization front would be of the type

$$\ddot{x} + h(t)\dot{x} = 0, \quad (24)$$

with a function h . This type of equation can be solved with an integrating factor

$$\mu(t) = \exp \int h(t) dt, \quad (25)$$

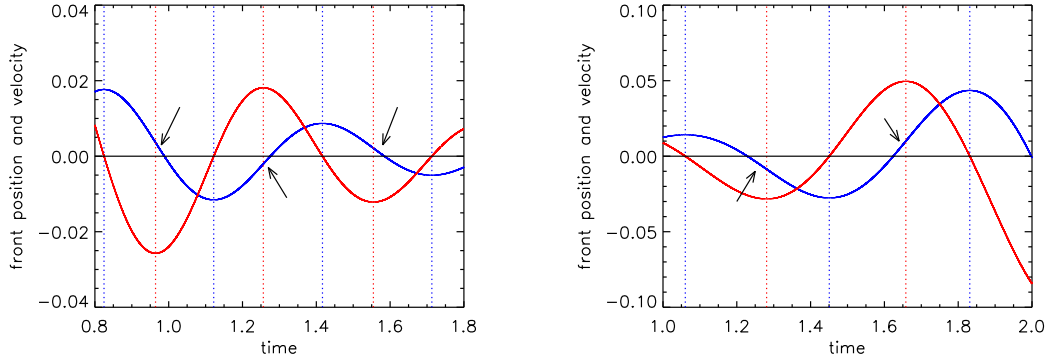


Figure 3. Details of Fig. 2. The arrows point to locations where it is easy to see that the change in the sign of the velocity does not occur exactly at the time that the position of the front reaches its maximum or minimum from equilibrium. In the case of damped oscillations (left-hand panel), the oscillations of velocity lag those in position. If the oscillations in velocity lead those in position (right-hand panel), the oscillations are amplified.

with the argument of the exponent setting a time-dependent damping or amplification time-scale. Of course, owing to the complexity of the equations for accretion, it is not possible to write a closed-form equivalent of the function, h , and therefore the differential equations for accretion cannot be solved in this way. None the less, because equations (21) and (23) are not of the same form, the dynamics of two-phase accretion are different from those of a non-linearly damped harmonic oscillator.

2.5.3 Comparison with pressure-driven expansion

In the textbook model for pressure-driven expansion of an H II region into a uniform, static gas (Spitzer 1978; Shu 1991), once the velocity of an R-type ionization front slows to its critical value, the ionization front transitions to a D-type with a preceding isothermal shock. In this model, the velocity of the front is consistent with ionization equilibrium as it is in the model for ionized accretion. However, the subsonic, pressure-driven expansion of the H II region determines the gas velocities across the shock and ionization fronts. In effect, the jump conditions depend on the velocities from the inside out. In contrast, in ionized accretion, the gas within the H II region is flowing inwards, almost in free fall, and hydrodynamic pressure is not effectively transmitted upstream. The jump conditions depend on the velocities from the outside inwards with the hydrodynamic pressure within the thin shell of post-shock neutral gas regulating the speed of the isothermal shock. In both models, when $u_{1f} < u_R$ and a double-front structure is required, the result is the same – the gas enters the H II region at the ionized sound speed with respect to the velocity of the ionization front.

3 NUMERICAL HYDRODYNAMIC SIMULATIONS

With the method of characteristics, we have described solutions of the coupled ODEs for the ionized gas that result in damped oscillations and conditionally stable oscillations for relative velocities above the R-critical limit, $\hat{u}_{1f} = u_R$, or as an approximation, not much below the limit. Following the same method, we could extend the ODE model to include relative velocities arbitrarily below the R-critical limit by adding an additional zone to our model to calculate the hydrodynamic evolution within the thin shell of post-shock neutral gas ahead of the ionization front when this shell develops as a result of the transition from an R-type to a D-type ionization front. This would be a second IVP to be solved as a BVP with the ionization front as the

inner boundary and the shock as the outer boundary. However, with sufficient understanding of the dynamics gained through the simplified physics described by the coupled ODEs of the two-zone model, a better course may be a change of method to follow the evolution with a finite-volume numerical hydrodynamical simulation.

3.1 Code

The hydrodynamical evolution for the full accretion flow, neutral and ionized, is followed using the open-source code PLUTO version 4.1 (Mignone et al. 2007) configured for one-dimensional (1D) simulations assuming spherical symmetry. The ionization-radiation transport is solved using the ray-tracing module SEDNA (Kuiper & Hosokawa 2018; Kuiper, Yorke & Mignone 2020). From the range of hydrodynamics solvers available in PLUTO, we use the HLLC scheme (Harten–Lax–Van Leer scheme including the contact discontinuity). With a WENO3 interpolation scheme in space and a Runge–Kutta 3 interpolation in time, the hydrodynamics are accurate to third order in space and time. The thermal equation of state of the gas is locally isothermal, with the actual gas temperature as a function only of the ionization fraction, ϵ ,

$$T_{\text{gas}} = \epsilon \times T_{\text{ion}} + (1 - \epsilon) \times T_{\text{neu}}. \quad (26)$$

3.2 Initial conditions

Our initial model is chosen to be similar to that of Vandenbroucke et al. (2019) with a fixed central mass, $M = 18 M_{\odot}$, neutral and ionized gas temperatures, $T_1 = 500$ K, $T_2 = 8000$ K, and the density at infinity normalized to $\rho_{\infty} = 10^{-19} \text{ g cm}^{-3}$. The neutral and ionized sound speeds are $a_1 = 2.03$ and $a_2 = 11.5 \text{ km s}^{-1}$, respectively. The Bondi radii [$GM/(2a^2)$] for the two phases are $R_{B1} = 1942$ and $R_{B2} = 60.5$ au, respectively.

At the outer boundary of the computational domain, $R_{\text{max}} = 100$ au, we set the gas mass density and gas velocity to the analytical solution of the Bondi accretion flow, specifically $\rho_{\text{gas}} \approx 2 \times 10^{-17} \text{ g cm}^{-3}$ and $v_{\text{gas}} \approx -16.6 \text{ km s}^{-1}$. At the inner boundary, R_{min} , we use zero-gradient boundary conditions, i.e. mass, momentum, and energy are allowed to stream freely across the boundary. The spatial resolution of the grid is uniform with $\Delta r = 1/30$ au. We ran simulations with two choices for $R_{\text{min}} = 10$ (same as Vandenbroucke et al. 2019), and also at 1 au.

To develop an initial accretion flow in equilibrium, we start with a uniform density, ρ_{gas} , equal to the value at 100 au, given above,

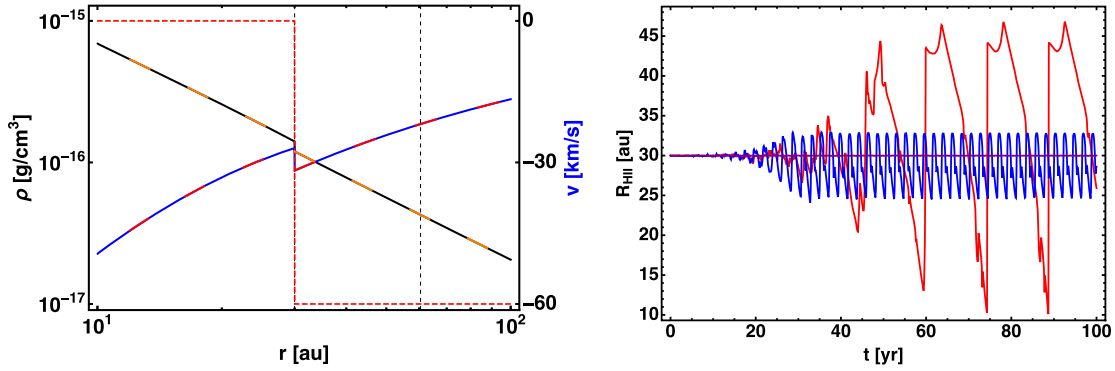


Figure 4. Left-hand panel: initial steady-state solution of the ionized Bondi accretion flow. Gas mass density (left-hand vertical axis) as a function of radius from the numerical simulation is shown as a black line overlain by an orange long-dashed line corresponding to the analytical solution. Gas velocity (right-hand vertical axis) as a function of radius from the numerical simulation is shown as a blue line overlain by a red long-dashed line corresponding to the analytical solution. The ionization fraction (dashed red line) jumps from 100 per cent to 0 per cent at the ionization front. Vertical dashed lines denote the location of the initial ionization front at 30 au and the Bondi radius with respect to the ionized gas temperature at ≈ 61.5 au. Two movies showing the evolution of gas mass density and gas velocity from the uniform initial condition towards the steady-state solution of the ionized Bondi accretion flow are available online. A first movie shows the evolution from the uniform initial conditions to the steady-state solution of the neutral Bondi accretion flow. A second movie shows the further evolution after the addition of the ionization front. In the movies, dashed lines denote the analytic solutions for the neutral and ionized flow, respectively. Right-hand panel: evolution of the location R_f of the ionization front. The position of the ionization front as a function of time is shown from the initial conditions (left-hand panel) for the exact equilibrium (horizontal black line at 30 au) and for a slight offset from equilibrium (red line) achieved by reducing the constant ionizing luminosity by -0.06 per cent of its equilibrium value. Also shown is the time evolution but with the ionized gas temperature reduced by a factor of 2 to 4000 K (blue line). Four movies showing the temporal evolution of the gas mass density and gas velocity profiles for ionized gas temperatures of 8000 (equilibrium and non-equilibrium), 4000, and 2000 K are also available online.

and a uniform temperature, T_1 , given above. As a first step, we let the system evolve without ionization under the gravitational influence of the constant central mass until the flow arrives at the single-phase Bondi transonic solution. In a second step, we add an ionization front at a fixed position (30 and 12 au, respectively, in our two examples discussed below). The velocity of the neutral flow along with the gas temperatures in the two phases defines the jump conditions at R_f . We evolve this system hydrodynamically (without radiation transport) until another steady state is reached. The ionizing luminosity required for equilibrium is then derived from the density profile inside of the ionization front along with the neutral flux through the front. We now have the initial equilibrium state (Fig. 4) for the fully time-dependent coupled hydrodynamic and photoionization-radiation transport problem.

3.3 Time-dependent evolution

We allow the position of the front to move in response to the ionizing flux at the front, which is calculated as the solution of the radiation transport problem. As shown in Fig. 4, the position of the front does not change from the initial equilibrium. However, the equilibrium is not stable. For example, if the ionizing luminosity is changed by -0.06 per cent and then held constant, the position of the front develops oscillations, shown in our Fig. 4, nearly identical to those found by Vandenbroucke et al. (2019, their figs 6 and 8). In this example, the front periodically reaches the inner boundary, resulting momentarily in a fully neutral accretion flow. The H II region immediately re-establishes itself with the position of the front in ionization equilibrium with the density profile of the neutral steady-state transonic Bondi solution. However, now the system is not in hydrodynamic equilibrium because compression through the front requires an ionized density profile consistent with a different energy constant, \mathcal{L} (equation 7).

This behaviour is not universal but dependent on the initial conditions. For example, reducing the ionized gas temperature to

4000 K results in a solution that is conditionally stable in that the maximum amplitude of the oscillations is limited, and the position of the front oscillates closely around the equilibrium position as seen in Fig. 4. If the ionized gas temperature is further reduced to 2000 K, the solution remains essentially the same as the equilibrium solution. The lower ratio of ionized to neutral sound speeds weakens the compression across the ionization front, which ultimately lengthens the response time of the ionization. In our ODE model, the relevant equations are (13)–(15).

Our non-dimensional ODE solution indicates that the differences in evolution are due to the differences in the compression of the gas at the H II region boundary, which is set by the temperature ratio. (Our non-dimensional solutions shown in Figs 2 and 3 have a temperature ratio of 100.) For any temperature ratio, solutions may be stable, conditionally stable, or unstable according to the initial position of the front with respect to the temperature-dependent Bondi radius. For lower temperature ratios, stable solutions are found within a wider range in the position of the front.

We next ran two series of simulations inserting a density perturbation in the neutral flow upstream of the ionization front. Each series includes perturbations of different amplitudes, one per simulation, with multiplicative factors between 10 and 0.001 of the neutral steady-state transonic density. The density perturbations all have a width of 5 au. The initial (equilibrium) position of the ionization front is 12 au, $x_c/x_f = 1/5$. The inner boundary is 10 au in the first series and 1 au in the second. The ionized and neutral temperatures are 8000 and 500 K, respectively, as in the original example.

Fig. 5 shows the results. Density perturbations of any amplitude result in oscillations of the position of the front. Density perturbations of larger amplitude result in an initial collapse of the H II region through the inner boundary. The collapse occurs as the initial perturbation is advected through the ionization front and the density-dependent recombination rate limits the number of ionizing photons reaching the front. Once a large-amplitude perturbation has been mostly advected through the inner boundary, the H II region is re-

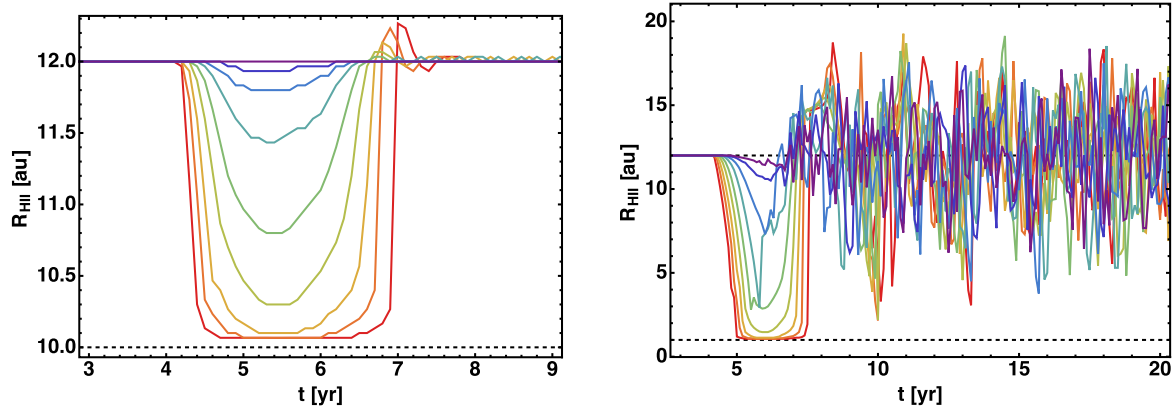


Figure 5. Temporal evolution of the location R_f of the ionization front, initially located at 12 au, for nine different initial perturbation strengths, 10.0, 3.0, 1.0, 0.3, 0.1, 0.03, 0.01, 0.003, and 0.001, times the steady-state transonic density, shown as colours on a rainbow scale ranging from red to blue, largest to smallest perturbation strengths, respectively. The dashed horizontal line at 12 au shows the initial (equilibrium) position of the ionization front. The inner boundary is 10 au in the example shown in the left-hand panel and 1 au in the example shown in the right-hand panel indicated by dashed lines. Two movies showing the temporal evolution of the gas mass density and gas velocity profiles are also available online (perturbations of 0.1 and inner boundaries of 10 and 1 au, respectively).

established, and the position of the front then oscillates around its equilibrium value. With the inner boundary at 10 au, the oscillations are damped resulting in a stable solution. With the inner boundary at 1 au, the oscillations are conditionally stable with limited growth in amplitude. Even after long evolutionary times (100 yr), these conditionally stable oscillations never result in subsequent collapse of the H II region. In these examples, the difference between the stable and conditionally stable behaviour is due to the lower degree of spherical compression with a larger inner radius resulting in more stable behaviour. If our non-dimensional ODE examples (Figs 2 and 3) were scaled to correspond to the dimensional initial conditions of these numerical simulations, the inner boundary in the ODE solutions would be 9.7 au.

4 ASTROPHYSICAL IMPLICATIONS

The astrophysical applications of the instabilities in spherical ionized accretion may be limited because of the dependence of the instability on the spherical geometry of Bondi accretion flow and specifically on the spherical convergence of the flow. Astrophysical accretion flows are generally flattened in geometry due to the conservation of angular momentum. While the density in these 2D, rotationally flattened flows is also expected to increase at smaller radii, the 2D geometry lacks the spherical compression of the 1D model because the compression can be relieved by expansion of the disc scale height. Oscillations seen in the spherical Bondi problem are not expected nor seen in 2D and 3D numerical simulations of rotationally flattened accretion flows with ionization (Kuiper & Hosokawa 2018; Sartorio et al. 2019).

5 CONCLUSIONS

The spherical convergence in Bondi accretion causes the density to increase rapidly at smaller radii, approximately as $r^{-1.5}$ (free fall). In a two-phase accretion flow, because the recombination rate increases as the square of the density, the effective opacity of the H II region and therefore the ionizing flux at the front is controlled predominately by the higher density region at smaller radii. The ionizing flux at the front controls the velocity of the front, which in turn determines the compression of the flow through the H II region boundary, and with

a time lag due to advection, the density at smaller radii. The offset of the phases of oscillations in the position and velocity of the front may lead to either damped or growing oscillation amplitudes. Amplitude growth may be limited by the transition of the ionization front from R-type to D-type and back as the transition limits the velocity of the front.

ACKNOWLEDGEMENTS

RK acknowledges financial support via the Emmy Noether and Heisenberg Research Grants funded by the German Research Foundation (DFG) under grant nos KU 2849/3 and 2849/9.

DATA AVAILABILITY

No new data were generated or analysed in support of this research.

REFERENCES

- Bondi H., 1952, *MNRAS*, 112, 195
- Keto E., 2002a, *ApJ*, 568, 754
- Keto E., 2002b, *ApJ*, 580, 980
- Keto E., 2007, *ApJ*, 666, 976
- Keto E., 2020, *MNRAS*, 493, 2834
- Kuiper R., Hosokawa T., 2018, *A&A*, 616, A101
- Kuiper R., Yorke H. W., Mignone A., 2020, *ApJS*, 250, 13
- Mestel L., 1954, *MNRAS*, 114, 437
- Mignone A., Bodo G., Massaglia S., Matsakos T., Tesileanu O., Zanni C., Ferrari A., 2007, *ApJS*, 170, 228
- Parker E. N., 1958, *ApJ*, 128, 664
- Sartorio N. S., Vandenbroucke B., Falceta-Goncalves D., Wood K., Keto E., 2019, *MNRAS*, 486, 5171
- Savedoff M. P., Greene J., 1955, *ApJ*, 122, 477
- Shu F., 1991, *Physics of Astrophysics, Vol. II: Gas Dynamics*. University Science Books, 648 Broadway, Suite 902, New York, NY
- Spitzer L., 1978, *Physical Processes in the Interstellar Medium*. Wiley, New York
- Vandenbroucke B. et al., 2019, *MNRAS*, 485, 3771

SUPPORTING INFORMATION

Supplementary data are available at *MNRAS* online.

Figure 4. Left-hand panel: initial steady-state solution of the ionized Bondi accretion flow.

Figure 5. Temporal evolution of the location R_f of the ionization front, initially located at 12 au, for nine different initial perturbation strengths, 10.0, 3.0, 1.0, 0.3, 0.1, 0.03, 0.01, 0.003, and 0.001, times the steady-state transonic density, shown as colours orange, yellow, light green, cyan blue, light blue, dark blue, and purple, respectively.

Please note: Oxford University Press is not responsible for the content or functionality of any supporting materials supplied by the authors. Any queries (other than missing material) should be directed to the corresponding author for the paper.

This paper has been typeset from a \TeX/L\AA\TeX file prepared by the author.